https://doi.org/10.15407/ujpe68.3.190

Y.M. AZHNIUK,[1] YE.O. HAVRYLIUK,[2,3,4] B.V. LOPUSHANSKA,[5]
V.V. LOPUSHANSKY,[1] A.V. GOMONNAI,[1,5] D.R.T. ZAHN[3,4]

[1] Institute of Electron Physics, Nat. Acad. Sci. Ukraine
(21, Universytetska Str., Uzhhorod 88017, Ukraine; e-mail: yu.azhniuk@gmail.com)
[2] V. Lashkaryov Institute of Semiconductor Physics, Nat. Acad. Sci. Ukraine
(45, Prospect Nauky, Kyiv 03028, Ukraine)
[3] Semiconductor Physics, Chemnitz University of Technology
(D-09107 Chemnitz, Germany)
[4] Center for Materials, Architectures and Integration of Nanomembranes (MAIN), Chemnitz University of Technology
(D-09107 Chemnitz, Germany)
[5] Uzhhorod National University
(3, Narodna Sq., Uzhhorod 88000, Ukraine)

STRUCTURAL AND OPTICAL CHARACTERISATION OF SIZE-SELECTED GLUTATHIONE-CAPPED COLLOIDAL Cu–In–S QUANTUM DOTS

Size-selected series of copper-deficient colloidal Cu–In–S quantum dots (QDs) stabilized with glutathione are obtained by the exchange reaction in aqueous solutions under mild synthesis conditions. The optical bandgap and photoluminescence maximum position shift toward higher energies with decreasing QD size. Based on X-ray diffraction data, the QDs are assigned to a tetragonal chalcopyrite-type structure. The average size of QDs, estimated from the Scherrer formula and from the comparison with the absorption edge-based sizing curves, exhibits a fair agreement, being in the interval of 1.2–2.9 nm. The Raman spectra of Cu–In–S QDs are analyzed with the account for the QD structure, confinement-related effects, non-stoichiometry, and possible existence of secondary phases.

K e y w o r d s: quantum dots, colloidal synthesis, optical absorption, photoluminescence, X-ray diffraction, Raman spectroscopy.

1. Introduction

Within the recent decade, the development of the methods of colloidal synthesis led to a family of ternary I–III–VI_2 semiconductor quantum dots (QDs) fabricated as a promising alternative to well-studied binary II–VI and IV–VI QDs [1–8]. The new materials appeared interesting and important not only in view of their "green" synthesis (without toxic cadmium- and lead-containing reagents), but also due to intense broadband luminescence in the visible spectral range and prospective applications in light-emitting diodes, photovoltaic solar cells, temperature sensors, biomedicine, and photocatalysis [1–8]. The QD family includes not only stoichiometric I–III–VI_2 (first of all, $CuInS_2$ and $AgInS_2$) semiconductors, but also group I element-deficient I–III–VI QDs which are known to exhibit even more intense photoluminescence (PL) with quantum yield reaching as high as 65–70 %, especially upon coating the QDs with a ZnS shell [9–11].

Colloidal I–III–VI QDs can be synthesized in organic media or aqueous media [7]. The first approach generally involves the pyrolysis of precursors in the presence of hydrophobic solvents and

Citation: Azhniuk Y.M., Havryliuk Ye.O., Lopushanska B.V., Lopushansky V.V., Gomonnai A.V., Zahn D.R.T. Structural and optical characterisation of size-selected glutathione-capped colloidal Cu–In–S quantum dots. *Ukr. J. Phys.* **68**, No. 3, 190 (2023). https://doi.org/10.15407/ujpe68.3.190.
Цитування: Ажнюк Ю.М., Гаврилюк Є.О., Лопушанська Б.В., Лопушанський В.В., Гомоннай О.В., Цан Д.Р.Т. Структурні й оптичні характеристики розподілених за розміром квантових точок Cu–In–S, вкритих глутатіоном. *Укр. фіз. журн.* **68**, № 3, 190 (2023).

capping agents/ligands at elevated temperatures in an inert atmosphere. It can be performed using the well-elaborated hot-injection [12], heating-up (non-injection) [13], thermal decomposition of a single-source precursor [14], tuning the relative reactivity of cationic precursors [15], or solvothermal [16, 17] techniques and leads to the formation of hydrophobic I–III–VI QDs. In order to obtain water-soluble QDs, important for applications in life sciences, the ligand exchange is performed [7]. A water-based approach is the direct synthesis from aqueous solutions by the arrested precipitation with mercaptoacetic (thioglycolic) acid [10, 18], mercaptopropionic acid [19], glutathione [11, 20], *etc.* acting as a stabilizer. These organic compounds contain an –SH group, by means of which they are bound to the QD surface, while carboxylic anion groups prevent the QD aggregation in the solution [2, 11, 21]. QDs obtained by water-based synthesis can be directly used for biological applications, but generally possess a lower luminescence efficiency (compared to the QDs obtained by the synthesis in organic media at higher temperatures) because of the QD surface oxidation [5].

In this work, we report on nonstoichiometric Cu–In–S QDs synthesised under mild conditions (below 100 °C) in aqueous solutions using glutathione (GSH) as a stabilizer. The QDs, fractionized for the size selection, are characterized by X-ray diffraction (XRD), optical absorption, PL, and Raman spectroscopy.

2. Experimental

Colloidal Cu–In–S QDs were synthesized in the exchange reaction between Na_2S and a mixture of Cu(II) and In(III) complexes in the desired proportions with glutathione (GSH) in alkaline (with addition of NH_4OH) aqueous solutions at a relatively mild temperature (96–98 °C) using an approach basically similar to the one described earlier [18, 22, 23]. In a typical synthesis process, we mixed 2.5 ml of deionized water with 2.4 ml of 0.5 M aqueous GSH solution and 0.8 ml of 1 M aqueous $InCl_3$ solution (with 0.05 ml of 0.2 M HNO_3). The mixture was kept at the constant stirring for 5 min. Then, 1 ml of 25% NH_4OH solution was added, after the 2-min stirring followed by the addition of 2 ml of 0.1 M aqueous $CuCl_2$ solution, and a quick addition of 1 ml of 1.0 M aqueous Na_2S solution and 0.25 ml of 2.0 M aqueous solution of citric acid resulting in the appearance of orange color. The whole procedure was performed at a constant magnetic stirring. Subsequently, the reaction mixture was heated in a water bath at 95 °C for 40 min producing a colloidal solution of intense red color. The total volume of the produced Cu–In–S QD solution was 10 ml.

The obtained crude QD solution was afterward subjected to the size fractioning by repeated centrifuging with addition, each time, of a new portion of a poor solvent (2-propanol C_3H_7OH), similarly to the procedure described earlier [10, 22, 23]. C_3H_7OH was added in portions of 0.4 ml to 4.0 ml of the QD solution obtained; then it was subjected to the centrifuging for 5 min at 4000 rpm expecting the precipitate to appear. As no precipitate was formed after the first centrifuging session, another 0.4 ml portions of C_3H_7OH were added followed by a repeated centrifuging of the same speed and duration. The first precipitate appeared after the fourth portion of C_3H_7OH (in total 2.0 ml). This precipitate was then separated and redissolved in deionized water producing the first fraction with the biggest QDs. This procedure (addition of 0.4 ml of 2-propanol to the remaining supernatant, centrifugation, and redissolution of the precipitate) was repeated several times, thereby leading to a series of five fractions with decreasing average QD size, visually changing their color from dark red to light yellow.

Measurements of optical absorption spectra of the size-selected QD colloidal solutions were carried out using a Cary 50 spectrophotometer (Varian) with a Xe pulse lamp source and dual Si diode detectors. PL spectra were measured using a Black Comet CXR-SR spectrometer (StellarNet) with diode excitation (λ_{exc} = 390 nm). Micro-Raman spectra were investigated using an XPloRa Plus (Horiba) spectrometer (2400 grooves/mm grating, cooled CCD camera) with the excitation by a λ_{exc} = 532 nm laser. The spectral resolution was better than 2.5 cm^{-1}. For XRD studies, a Rigaku Smartlab operating with Cu K_α radiation (λ = 1.54056 Å) was employed. The measurements were performed using Bragg–Brentano and parallel-beam configurations. For the micro-Raman and XRD measurements, Cu–In–S QDs colloidal solutions were drop-casted onto a silicon substrate and dried at room temperature in a fume hood. All measurements were performed at room temperature.

3. Results and Discussion

Optical absorption spectra of size-selected GSH-capped Cu–In–S QD solutions obtained at the molar precursor ratio [Cu] : [In] : [S]=1 : 4 : 5 are shown in Fig. 1, *a*. The absorption edge is seen to shift noticeably toward higher energies with increasing fraction number, thus being the evidence of a QD size decrease. The results obtained are in agreement with data reported earlier for size-selected $CuInS_2$ QDs synthesized by thermal decomposition of a single-source precursor [14], tuning the relative reactivity of cationic precursors [15], solvothermal [16, 17] and hydrothermal [24] methods. Note that, in our case, the technique enabled the QD ensemble to be separated in a larger number of size-selected fractions than in the quoted studies. Meanwhile, the optical absorption spectra for fractions 4 and 5 in the high-energy region look rather untypical, which implies the possible presence of residual by-products in these fractions.

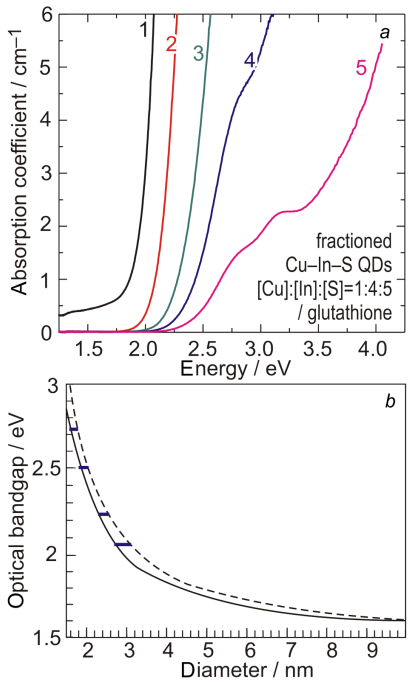

Fig. 1. Optical absorption spectra of size-selected GSH-capped Cu–In–S QD solutions obtained at molar precursor ratio [Cu] : [In] : [S] = 1 : 4 : 5 (*a*). Comparison of the E_g values obtained here from the optical absorption spectra of the Cu–In–S QD size-selected fractions (blue bars) with the sizing curve. The dashed line shows calculations in the effective-mass approximation, and the solid line is based on the analytical ultracentrifugation data for $CuInS_2$ QDs with the account for optical absorption and photoluminescence excitation spectra [17] (*b*)

Optical absorption spectra of a similar kind were reported in a number of studies for colloidal Cu–In–S QDs synthesized at elevated temperatures (solvothermal and hydrothermal techniques, hot-injection, *etc.*) [1, 9, 24–27], as well as obtained in aqueous solutions at mild temperatures using GSH [20, 28] or mercaptoacetic acid [18] as a stabilizer. Note that, in the quoted studies, no size fractioning of the colloidal QDs was performed. Hence, the absorption spectra of their samples were determined by the absorption of the largest QDs present in the colloidal solution. Obtaining QDs with different absorption edge positions (different bandgaps) was achieved either by a variation of the reaction temperature [14, 15, 24, 25] or the duration [16, 17, 25], or by changing the [Cu] : [In] precursor concentration ratio [1, 20, 24–26]. A variation of the latter resulted in the fabrication of stoichiometric and near-stoichiometric $CuInS_2$ QDs [14–17, 24–27] or non-stoichiometric, mostly copper-deficient [18, 20, 24, 26, 28], but sometimes also copper-enriched [24] Cu–In–S nanoparticles.

Note that $CuInS_2$ is a direct-bandgap semiconductor with E_g = 1.45 eV and a high extinction coefficient in the visible spectral range, what makes it a promising material for the solar energy conversion. The exciton Bohr radius for $CuInS_2$ is 4.1 nm; therefore, confinement-related effects in the optical spectra of $CuInS_2$ nanocrystals should be observed for their size below about 8 nm [1]. Unlike the absorption spectra of II–VI QDs, for which distinct size-dependent maxima are observed for narrow-dispersion ensembles of QDs (in the case where their size is below the exciton Bohr radius) enabling the QD size to be determined within the effective mass approximation [29–31]. For Cu–In–S QDs, we did not observe any confinement-related maxima. The maxima can be smeared by the strong Urbach tail absorption on defect states, which are highly probable in non-stoichiometric low-dimensional compounds of this family [10]. Spectra of a similar kind are also well known for Ag–In–S QDs [11, 22, 23]. However, the absorption spectra of Hg–In–S colloidal QDs of the same family prepared and fractioned by a similar technique exhibited size-dependent maxima [32].

As the absorption edge of Cu–In–S QDs is formed by direct optical transitions, one can determine the bandgap value E_g for each fraction from the absorp-

tion spectra plotted in the so-called Tauc coordinates ($(\alpha h\nu)^2$ versus $h\nu$) by approximating the extended linear section of the relevant plot to intercept the abscissa axis. The corresponding values are listed in Table.

As is seen from Fig. 1, *a*, with Cu–In–S QD size variation, their absorption edge position can vary in a broad spectral interval. Calculations in the effective-mass approximation performed for $CuInS_2$ QDs in the size interval from 1 to 6 nm showed that E_g in this case varies from 3.3 to 1.7 eV, which is in a good agreement with the experimental data [1]. Based on calculations and experimental data, several groups have obtained the so-called sizing curves to determine the average size of $CuInS_2$ nanoparticles from the E_g value derived from the absorption spectra [15, 17, 27]. We compared the E_g values determined from the absorption spectra in Fig. 1, *a* (see Table) to the sizing curves from the quoted studies (Fig. 1, *b*). Thus estimated average size values for the synthesized Cu–In–S QD fractions are given in the last column of Table. Note that the sizing curve reported in the earlier study [15] encompasses a too narrow interval to be compared to our data, while the sizing curves from more recent studies [17, 27] show a quite good agreement with each other. The data quoted in Table for the first four Cu–In–S QD fractions are obtained by comparison with the sizing curve [17] which covers the broadest spectral interval. The determined average size values for the first four fractions basically correlate with the data of other authors [18] who used a similar approach for the Cu–In–S QD fabrication and combined the optical absorption studies with other techniques to determine the QD size. The E_g value for fraction 5 (see Fig. 1, *a* and Table) is quite beyond the results of other authors [17, 27], and it is probable that this fraction is formed not (not only) by the smallest Cu–In–S QDs.

The Cu–In–S QDs obtained are characterized by broadband luminescence, although it is less intense than for Ag–In–S QDs prepared earlier by a similar method [22, 23]. The first fractions with larger QDs do not exhibit noticeable PL, while, for the fractions from 3 to 5, it increases in intensity and shifts toward shorter wavelengths (higher energies), as can be seen from Fig. 2. The PL maximum energy positions and Stokes shift values are shown in Table. Note that earlier studies of PL in Cu–In–S QDs also reported rather broad emission bands, sometimes composed of

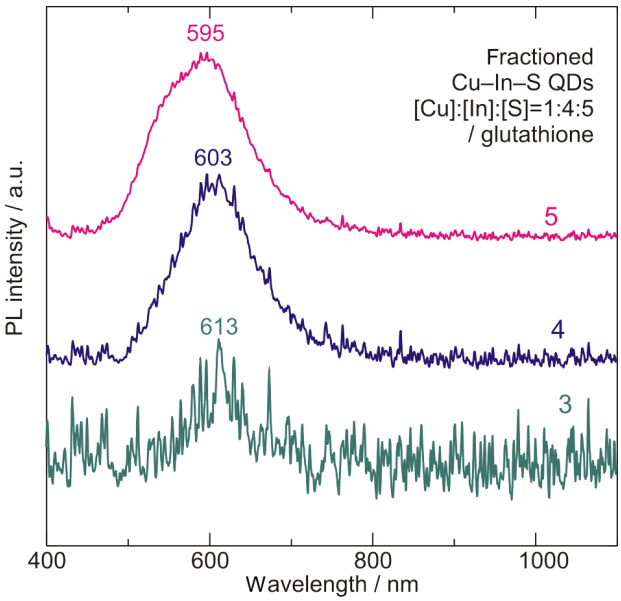

Fig. 2. PL spectra of size-selected fractions GSH-capped Cu–In–S QD solutions obtained at molar precursor ratio [Cu] : [In] : [S]=1 : 4 : 5

two overlapping maxima [33], and a quite noticeable Stokes shift [1].

In earlier studies, the emission in Cu–In–S QDs was assigned to the donor–acceptor (D–A) pair recombination [14, 33, 34], with the copper vacancy being an acceptor state, whereas the sulfur vacancy or the copper indium substitution acting as a donor. In view of this, increasing the amount of copper vacancies (copper deficiency) was an efficient way to increase the emission quantum yield [1, 34]. Meanwhile, Hamanaka *et al.* [35] attributed the PL in Cu-

Energy bandgap E_g, PL maximum energy position E_{PL}, Stokes shift Δ_S and average size d evaluated from the optical absorption spectra of size-selected fractions of GSH-capped Cu–In–S QDs obtained at the precursor ratio [Cu] : [In] : [S] = 1 : 4 : 5 in the reaction mixture

Fraction No.	E_g, eV	E_{PL}, eV	Δ_S, eV	d, nm
1	2.05	–	–	2.9 ± 0.3
2	2.23	–	–	2.4 ± 0.2
3	2.51	2.02	0.49	2.0 ± 0.2
4	2.73	2.06	0.67	1.7 ± 0.2
5	3.92	2.08	1.84	–

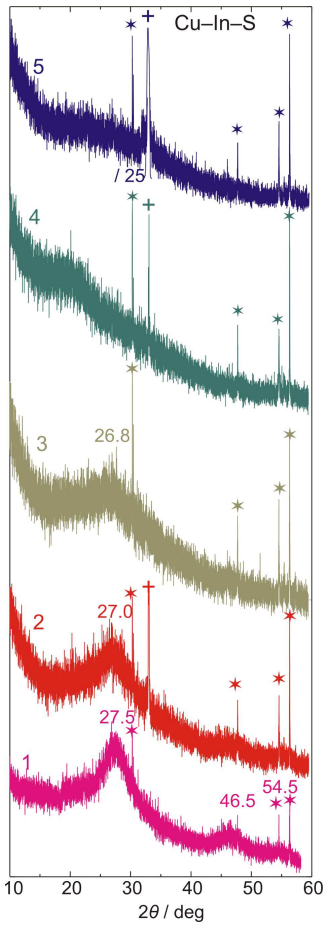

Fig. 3. X-ray diffractograms of size-selected fractions of Cu–In–S QDs obtained with the precursor molar ratio [Cu] : [In] : [S] = 1 : 4 : 5. Asterisks denote reflexes from the substrate (Si), crosses (+) – from the exchange reaction by-product(NaCl)

deficient Cu–In–S QDs to the recombination of electrons and holes trapped in the deep surface defect states, rather than to D–A transitions between intrinsic defects.

An alternative model of self-trapped excitons was proposed, for which one of the photogenerated carriers is localized at a certain lattice site, leading to a lattice distortion and a strong electron-phonon interaction. In this case, the broadband PL is explained as a series of phonon replicas of the pure excitonic (zero-phonon) emission line [8, 9, 36, 37]. Thus, the broadband PL is considered to arise from the whole QD lattice, not from individual defects. Tailoring the QD structure then enables high quantum yields to be achieved. According to this model, the broadband PL is a characteristic of individual QDs rather than the QD ensemble.

X-ray diffractograms obtained for the size-selected Cu–In–S QD fractions are illustrated by Fig. 3. Besides narrow peaks corresponding to reflexes from the silicon substrate and (for some fractions) the exchange reaction by-product NaCl, the XRD pattern of fraction 1 (the biggest nanoparticle size) contains much broader bands with maxima at 27.5°, 46.5°, and 54.5°. Similar broad bands were observed in XRD studies of Cu–In–S QDs with the average size of 2–4 nm performed by other authors [1, 13, 14, 17, 20, 25]. Note that, for bigger $CuInS_2$ nanoparticles (10–15 nm) noticeably narrower maxima at the same 2θ angles are observed, corresponding to reflexes from (112) ($2\theta = 27.5°$), (220) ($2\theta = 46.5°$), (312) ($2\theta = 54.5°$) planes of tetragonal (chalcopyrite-type) structure [27, 38, 39]. In our case for the biggest QDs (fraction 1), the halfwidth (FWHM) of the XRD maximum at $2\theta = 27.5°$ is 4.7° (Fig. 3). The large width of the XRD peaks is caused by small sizes of the QDs and encumbers unambiguous determination of the QD structure. The known Scherrer equation [40] enables the average size of the Cu–In–S QDs, L, to be evaluated from the FWHM of the (112) diffraction peak β:

$$\beta(2\theta) = K\lambda/L\cos\theta, \qquad (1)$$

where λ is the X-ray wavelength ($\lambda = 0.154$ nm) and K is the shape factor ($K = 0.9$). For fraction 1, the thus evaluated average QD size is 1.7 nm. With increasing the fraction number (decreasing nanoparticle size), the features in the diffractograms broaden, the signal-to-noise ratio worsens due to the QD size decrease, as well as to the smaller amount of nanoparticles in the higher fractions. In particular, for fraction 2, the above named peak FWHM is 6.5°. According to the Scherrer equation, this corresponds to the average QD size of 1.2 nm. For fraction 3, it is practically impossible to determine the halfwidth of the maximum (Fig. 3). But, for fractions with higher numbers (smaller QD size), a very broad smeared maximum can be observed closer to 20° (Fig. 3). Note that we earlier observed a similar broad feature for the smallest-size fractions of Ag–Ga–S QDs synthesized by the same technique [65]. This maximum can be related to by-products or unreacted complexes with GSH ligands.

It should be noted that the values of the average Cu–In–S QD size derived from the XRD peak halfwidths for the first two fractions in general agree with those obtained by other authors for Cu–In–S nanoparticles with similar characteristics [14, 17]. One should take into account that these values are close to the limit of the Scherrer equation applicability for the crystallite size evaluation. Hence, it is reasonable to compare the average size values to those determined from other independent measurements, in particular, transmission electron microscopy (TEM), similarly to how it was done by Akdas *et al.* [17]. Comparison of the results obtained here for the Cu–In–S QDs and based on the XRD data (1.7 nm and 1.2 nm for fractions 1 and 2, respectively) and on the optical absorption-based sizing curve [17] (2.9 nm and 2.4 nm for fractions 1 and 2, respectively, see Table) shows a reasonable discrepancy. Since both methods do not provide high accuracy and reliability, the real average size of the Cu–In–S nanoparticles is most likely within these limits (1.7–2.9 nm for fraction 1 and 1.2–2.4 nm for fraction 2). Note that discrepancies of a quite similar scale were obtained for the average size of $CuInS_2$ QDs determined from XRD, TEM, and optical absorption [17].

The micro-Raman spectrum of GSH-capped Cu–In–S QDs (fraction 2) is shown in Fig. 4. Note that there are quite numerous publications in the literature with regard for the Raman studies of Cu–In–S QDs [12, 13, 25, 28, 34, 38, 39, 41–45], as well as polycrystalline $CuInS_2$ films [46–49]. However, for bulk $CuInS_2$ crystals, the Raman studies are quite scarce and rather incomplete [50–53]. The Raman measurements of $CuInS_2$ QDs with the orthorhombic structure and with the average size of about 15 nm [12] revealed a rich Raman spectrum with rather narrow well resolved bands in the interval 70–350 cm^{-1}. Smaller-size nanoparticles, mostly with the tetragonal structure, similarly to our case, demonstrate broader, often overlapping bands [13, 25, 28, 34, 38, 41–45, 54]. The broadening and asymmetry of features in the Raman spectra of small nanocrystals is, in particular, due to the phonon confinement-related scattering by nonzero-wavevector phonons, as well as surface phonon scattering [55, 56]. In a number of cases, some bands can be masked or smeared, and the intensity ratio can vary among different studies. Note that some studies do not present Raman spectra measured below 200 cm^{-1} [13, 34, 41, 43] thereby

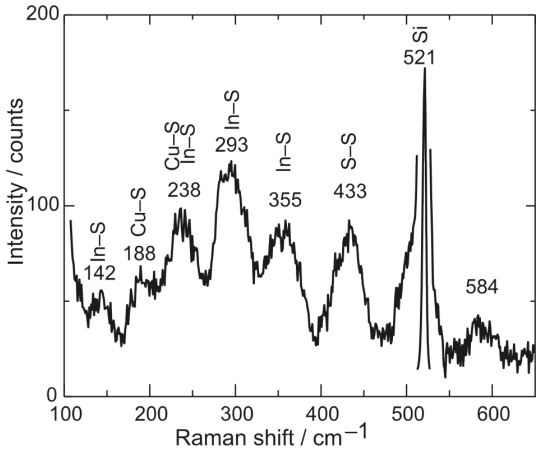

Fig. 4. Micro-Raman scattering spectrum of Cu–In–S/GSH QDs (fraction 2) measured at $\lambda_{exc} = 532$ nm

encumbering the comparison of the data. No major differences in the Raman spectra of stoichiometric ($CuInS_2$) and nonstoichiometric Cu–In–S nanoparticles are observed. However, the studies devoted to the effect of the [Cu] : [In] precursor concentration on the Raman spectra showed a redistribution of band intensities related to the participation of copper and indium cations in the corresponding vibrations [13, 34].

The lowest-frequency maximum is observed near 142 cm^{-1} (Fig. 4). For Cu–In–S QDs, a Raman peak at a relatively close frequency (123 cm^{-1}) was reported only in one of the earlier studies [28]. Meanwhile, the peak near 130–140 cm^{-1} was observed for $CuInS_2$ thin films [46, 48, 49] and bulk crystals [53]. A Raman feature in the same frequency region is known for In_2S_3 films [49]. Hence, it appears most likely to be due to In–S bond vibrations.

The Raman feature observed in Fig. 4 at 188 cm^{-1} was reported in several earlier studies of Cu–In–S QDs [25, 28, 45] and films [46]. It can be reasonably related to Cu–S bond vibrations, since it was clearly observed to shift from 190 cm^{-1} toward lower frequencies at the gradual Cu→Ag substitution in (Cu, Ag)–In–S QDs [28] exhibiting a one-mode behavior (for Ag–In–S QDs, the corresponding feature is seen at 170–180 cm^{-1} and related to Ag–S bond vibrations [22, 23, 28]). Likewise, it seems reasonable to relate the band at 238 cm^{-1} (Fig. 5) to Cu–S bond vibrations, since, in the spectra of the mixed (Cu,Ag)–In–S QDs, a feature observed as a shoulder at a somewhat higher frequency of 256 cm^{-1} also shifts toward lower frequencies at the Cu → Ag substitution [28]. The fea-

ture near 240–250 cm^{-1} is also reported for Cu–In–S QDs [38, 41, 43] and polycrystalline films [48, 57], while, in other studies, it was revealed as a shoulder near 260 cm^{-1} [42, 44, 45]. Sugan *et al.* reported on two distinct peaks at 233 and 269 cm^{-1} [39], but those measurements were performed for $CuInS_2$ nanocubes with the size of nearly 100 nm, for which the effect of phonon confinement and surface phonons [55] on the Raman spectra was minimal, unlike our case of much smaller nanoparticles. Similarly, two clear peaks near 240 and 260 cm^{-1} were observed for $CuInS_2$ thin films with the grain size much larger than the size of the QDs studied here. Still, the assignment of the observed feature in this spectral region mostly to Cu–S vibrations would be too simplified. As intense Raman peaks in this region are known for In_2S_3 thin films [49] and bulk crystals [58], we find it reasonable to assume that both Cu–S and In–S vibrations contribute to the Raman scattering in this spectral region, and the character of their overlapping not only depends on the [Cu] : [In] ratio in the nanoparticles, but is also determined by the QD size-governed contributions of confinement-related nonzero-wavevector phonons and surface phonons.

The most intense Raman feature in the spectra of tetragonal Cu–In–S QDs, observed near 290–300 cm^{-1}, is related to the vibrations of A_1 symmetry [25, 38, 39, 43, 45]. While, for the chalcopyrite-type structure, its maximum is seen near 291–298 cm^{-1} [38, 39, 43, 45], the CuAu-type structural modification is known to be characterized by a peak of the so-called A_1^* symmetry near 305 cm^{-1} [45, 47]. In our case, the observed peak at 293 cm^{-1} indicates the predominance of the chalcopyrite-type modification (Fig. 4), while its relatively broad halfwidth can be explained not only by a possible contribution of CuAu-type QDs, but also by the small QD size-related effects of confinement-related nonzero-wavevector phonons and surface phonons mentioned above. Note that the deconvolution of the first-order Raman spectrum of Cu–In–S QDs performed in the recent publication [45] shows a quite ample set of 11 oscillators which is consistent with DFT calculations for stoichiometric $CuInS_2$ [12]. Still, evidently, it cannot be considered ultimate for our case of nonstoichiometric QDs, especially in view of their extremely small size.

At a higher frequency, a somewhat weaker and broader peak is observed at 355 cm^{-1} (Fig. 4). Features in this frequency region, despite the fluctuations in the exact positions of the maxima, are in general reported for Cu–In–S QDs. Depending on the intensity of the maximum, this higher-frequency feature either appears as a shoulder of the dominating A_1 peak [34, 38, 41, 43, 44], or forms a continuum-like structure with a nearly flat maximum [13, 28, 45], or, similarly to ours, demonstrates a stronger maximum at 290–300 cm^{-1} and a well-separated higher-frequency one near 330–350 cm^{-1} [25]. The higher-frequency maximum at 330–350 cm^{-1} is either related to vibrations of Cu vacancy defects [25, 34] or interpreted as a combination of B_2- and E-symmetry vibrations of the $CuInS_2$ lattice [43]. An important issue arising while discussing the Raman spectra of Cu–In–S QDs is the possible presence of different $CuInS_2$ phases, as well as (especially for Cu-deficient QDs) the nanocrystalline $CuIn_5S_8$ phase and In_2S_3 phase [45, 49]. It is known that $CuIn_5S_8$ is characterized by intense Raman peaks in the interval 320–340 cm^{-1} [49], slightly below the maximum observed in the present study. It was also reported that, for Cu–In–S films, the intensity of the Raman feature in this region noticeably increases with deviation from the stoichiometric $CuInS_2$ composition toward the copper deficiency [49], which supports the assignment of this feature to Cu vacancy defects [25, 34]. Therefore, as well as in view of the fact that the Raman spectrum of In_2S_3 also contains features in this frequency interval (320 and 370 cm^{-1}) [59], we can assume that the observed band centered near 355 cm^{-1} is mostly related to In–S bond vibrations. On the other hand, a detailed analysis of the data available for Cu–In–S QDs and films ascribes the Raman feature at 340–350 cm^{-1} to a combination of LO modes of E and B_2 symmetries of the tetragonal-like structure distorted by the QD off-stoichiometry which can also be responsible for the activation of phonon modes that are not Raman-active in the ideal tetragonal lattice, as well as for changing the relative intensities of the Raman-active modes [45]. In our opinion, the QD lattice is distorted not only by the deviation from the stoichiometric composition, but also by the tiny QD size which makes the clear identification of their crystal structure, as well as the phonon band symmetry assignment, more ambiguous.

A rather intense broad band with the maximum at 433 cm^{-1} (Fig. 4) was not observed earlier for copper-deficient Cu–In–S QDs [28, 45], although, in some studies of stoichiometric or indium-deficient

samples, a Raman feature in this spectral region was reported. Namely, the noticeable maximum of a similar width and intensity was observed near 410 cm^{-1} for colloidal $CuInS_2$ QDs [25]. We note that, in the earlier study [41], a weak maximum near 430 cm^{-1} was observed. A similar band appeared in the Raman spectra of copper-rich Cu–In–S films ([Cu] : [In]=1.39) [49] and polycrystalline stoichiometric $CuInS_2$ films [57]. A weak band near 420 cm^{-1} is also known for orthorhombic $CuInS_2$ QDs [12, 54]. Note that a relatively broad band near 435 cm^{-1} was reported to be in the Raman spectra of quaternary Cu–Zn–Sn–S QDs, where it is related to the formation of secondary phases of Cu_xS type [54, 60]. In such case, it is understandable why this band was not observed in most of the Raman studies of stoichiometric or copper-deficient Cu–In–S QDs. Unexpectedly in our case, it is revealed in spite of no copper excess being expected in the synthesized QDs from the preparation procedure. A possible reason can be a partial degradation of Cu–In–S QDs in the colloidal solution leading to the reaction products with excessive copper content. In our case, we cannot exclude the formation of such phases upon ageing. In particular, our experiments on the synthesis of less copper-deficient Cu–In–S QDs (precursor ratio [Cu] : [In] : [S]=1 : 2 : 5) led to unstable colloidal solutions degrading with the formation of Cu_xS-type phases with distinct Raman features at 437 and 473 cm^{-1}. On the other hand, it is known that, for various sulphide materials, especially in disordered systems [61, 62], a band attributed to homopolar S–S vibrations is known to be observed in the frequency imterval 430–490 cm^{-1}. In particular, it was reported in the earlier studies of colloidal $AgInS_2$ QDs obtained by a similar method as a broad band near 450 cm^{-1} [63, 64].

4. Conclusions

Colloidal Cu–In–S QDs stabilized with GSH are obtained by the exchange reaction in aqueous solutions with molar precursor ratio [Cu] : [In] : [S]=1 : 4 : 5 under mild synthesis conditions. Size-selected fractions of the colloidal solutions exhibit a clearly size-dependent absorption edge, while confinement-related features in the absorption spectra are smeared by Urbach tails. The average QD size estimated from the comparison of the bandgap values with the known sizing curve [17] gradually varies from 2.9 to 1.7 nm for fractions from 1 to 4. Broadband PL is observed only for QD fractions with medium and smaller QD size, the PL intensity and maximum position increasing as the QD size decreases.

XRD data show broad reflexes for the first three Cu–In–S QD fractions, the XRD maximum position corresponding to the tetragonal chalcopyrite-type structure. The average size of QDs in the first two fractions, determined from the Scherrer equation, is underestimated in comparison with that estimated from optical absorption data, which is most likely related to a limited accuracy of the Scherrer equation for such small QD size.

The Raman spectra of QDs show a fair agreement with the data reported for stoichiometric and Cu-deficient Cu–In–S QDs with chalcopyrite-type structure. The clear identification of all vibrational features is encumbered by the small QD size resulting in the increasing contribution of surface phonons and the phonon confinement, as well as the sample non-stoichiometry, ambiguities in the symmetry assignment, and possible existence of secondary phases.

We are indebted to O.E. Raievska and O.L. Stroyuk for the helpful advice and discussion and to O.V. Selyshchev for the valuable discussion and critical comments to the manuscript. We appreciate the software assistance provided by M.V. Khoma. Y.M. Azhniuk is grateful to Chemnitz University of Technology for the financial support of his research visit to the University. Ye.O. Havryliuk is grateful to Alexander von Humboldt Foundation for funding his research and stay in TU Chemnitz.

1. J. Kolny-Olesiak, H. Weller. Synthesis and application of colloidal $CuInS_2$ semiconductor nanocrystals. *ACS Appl. Mater. Interfaces* **5**, 12221 (2013).
2. P. Reiss, M. Carriere, C. Lincheneau, L. Vaure, S. Tamang. Synthesis of semiconductor nanocrystals, focusing on nontoxic and earth-abundant materials. *Chem. Rev.* **116**, 10731 (2016).
3. G. Xu, S. Zeng, B. Zhang, M.T. Swihart, K.T. Yong, P.N. Prasad. New generation cadmium-free quantum dots for biophotonics and nanomedicine. *Chem. Rev.* **116**, 12234 (2016).
4. W.M. Girma, M.Z. Fahmi, A. Permadi, M.A. Abate, J.-Y. Chang. Synthetic strategies and biomedical applications of I–III–VI ternary quantum dots. *J. Mater. Chem. B* **5**, 6193 (2017).
5. O. Yarema, M. Yarema, V. Wood. Tuning the composition of multicomponent semiconductor nanocrystals: The case of I–III–VI materials. *Chem. Mater.* **30**, 1446 (2018).

6. Y. Liu, F. Li, H. Huang, B. Mao, Y. Liu, Z. Kang. Optoelectronic and photocatalytic properties of I–III–VI QDs: Bridging between traditional and emerging new QDs. *J. Semicond.* **41**, 091701 (2020).
7. O.S. Oluwafemi, E.H.M. Sakho, S. Parani, T.C. Lebepe. *Ternary Quantum Dots: Synthesis, Properties, and Applications* (Woodhead Publishing, 2021) [ISBN: 978-0-12-818304-5].
8. O. Stroyuk, O. Raievska, D.R.T. Zahn. Unique luminescent properties of composition-/size-selected aqueous Ag–In–S and core/shell Ag–In–S/ZnS quantum dots. In: *Core/Shell Quantum Dots*. Edited by X. Tong, Z. M. Wang (Springer, 2020) [ISBN: 978-3-030-46596-4].
9. K.E. Knowles, K.H. Hartstein, T.B. Kilburn, A. Marchioro, H.D. Nelson, P.J. Whitham, D.R. Gamelin. Luminescent colloidal semiconductor nanocrystals containing copper: synthesis, photophysics, and applications. *Chem. Rev.* **116**, 10820 (2016).
10. A. Raevskaya, V. Lesnyak, D Haubold, V. Dzhagan, O. Stroyuk, N. Gaponik, D.R.T. Zahn, A. Eychmüller. A fine size selection of brightly luminescent water-soluble Ag–In–S and Ag–In–S/ZnS quantum dots. *J. Phys. Chem. C* **121**, 9032 (2017).
11. O. Stroyuk, A. Raevskaya, F. Spranger, O. Selyshchev, V. Dzhagan, S. Schulze, D.R.T. Zahn, A. Eychmüller. Origin and dynamics of highly efficient broadband photoluminescence of aqueous glutathione-capped size-selected Ag–In–S quantum dots. *J. Phys. Chem. C* **122**, 13648 (2018).
12. V.M. Dzhagan, A.P. Litvinchuk, M. Ya. Valakh, M. Kruszynska, J. Kolny-Olesiak, C. Himcinschi, D.R.T. Zahn. Raman scattering in orthorhombic $CuInS_2$ nanocrystals. *Phys. Status Solidi A* **211**, 195 (2014).
13. N.T.M. Thuy, T.T.K. Chi, U.T.D. Thuy, N.Q. Liem. Low-cost and large-scale synthesis of $CuInS_2$ and $CuInS_2$/ZnS quantum dots in diesel. *Opt. Mater.* **37**, 823 (2014).
14. S.L. Castro, S.G. Bailey, R.P. Raffaelle, K.K. Banger, A.F. Hepp. Synthesis and characterization of colloidal $CuInS_2$ nanoparticles from a molecular single-source precursor. *J. Phys. Chem. B* **108**, 12429 (2004).
15. R Xie, M. Rutherford, X. Peng. Formation of high-quality I–III–VI semiconductor nanocrystals by tuning relative reactivity of cationic precursors. *J. Am. Chem. Soc.* **131**, 5691 (2009).
16. D.-E. Nam, W.-S. Song, H. Yang. Facile, air-insensitive solvothermal synthesis of emission-tunable $CuInS_2$/ZnS quantum dots with high quantum yields. *J. Mater. Chem.* **21**, 18220 (2011).
17. T. Akdas, J. Walter, D. Segets, M. Distasoa, B. Winter, B. Birajdar, E. Spiecker, W. Peukert. Investigation of the size-property relationship in $CuInS_2$ quantum dots. *Nanoscale* **7**, 18105 (2015).
18. A. Raevskaya, O. Rosovik, A. Kozytskiy, O. Stroyuk, V. Dzhagan, D.R.T. Zahn. Non-stoichiometric Cu–In–S/ZnS nanoparticles produced in aqueous solutions as light harvesters for liquid-junction photoelectrochemical solar cells. *RSC Adv.* **6**, 100145 (2016).
19. X. Yan, H. Li, Y. Yan, X. Su. Selective detection of parathion-methyl based on near-infrared $CuInS_2$ quantum dots. *Food Chemistry* **173**, 179 (2015).
20. M. Jiao, X. Huang, L. Ma, Y. Li, P. Zhang, X. Wei, L. Jing, X. Luo, A. L. Rogach, M. Gao. Biocompatible off-stoichiometric copper indium sulfide quantum dots with tunable near-infrared emission via aqueous based synthesis. *Chem. Commun.* **55**, 15053 (2019).
21. L. Jing, S.V. Kershaw, Y. Li, X. Huang, Y. Li, A.L. Rogach, M. Gao. Aqueous based semiconductor nanocrystals. *Chem. Rev.* **116**, 10623 (2016).
22. B.V. Lopushanska, Y.M. Azhniuk, V.V. Lopushansky, S.B. Molnar, I.P. Studenyak, O.V. Selyshchev, D.R.T. Zahn. Synthesis from aqueous solutions and optical properties of Ag–In–S quantum dots. *Appl. Nanosci.* **10**, 4909 (2020).
23. B.V. Lopushanska, Y.M. Azhniuk, D. Solonenko, V.V. Lopushansky, I.P. Studenyak, D.R.T. Zahn. Structural and optical study of glutathione-capped Ag–In–S nanocrystals. *Molec. Cryst. Liquid. Cryst.* **717**, 98 (2021).
24. C.I.L. Santos, W.S. Machado, K.D. Wegner, L.A.P. Gontijo, J. Bettini, M.A. Schiavon, P. Reiss, D. Aldakov. Hydrothermal synthesis of aqueous-soluble copper indium sulfide nanocrystals and their use in quantum dot sensitized solar cells. *Nanomaterials* **10**, 1252 (2020).
25. R.C. Fitzmorris, R.P. Oleksak, Z. Zhou, B.D. Mangum, J.N. Kurtin, G.S. Herman. Structural and optical characterization of $CuInS_2$ quantum dots synthesized by microwave-assisted continuous flow methods. *J. Nanopart. Res.* **17**, 319 (2015).
26. G. Wang, H. Wei, J. Shi, Y. Xu, H. Wu, Y. Luo, D. Li, Q. Meng. Significantly enhanced energy conversion efficiency of $CuInS_2$ quantum dot sensitized solar cells by controlling surface defects. *Nano Energy* **35**, 17 (2017).
27. C. Xia, W. Wu, T. Yu, X. Xie, C. Oversteeg, H.C. Gerritsen, C.M. Donega. Size-dependent band-gap and molar absorption coefficients of colloidal $CuInS_2$ quantum dots. *ACS Nano* **12**, 8350 (2018).
28. O. Raievska, O. Stroyuk, Y. Azhniuk, D. Solonenko, A. Barabash, C.J. Brabec, D.R.T. Zahn. Composition-dependent optical band bowing, vibrational and photochemical behavior of aqueous glutathione-capped (Cu,Ag)–In–S quantum dots. *J. Chem. Phys. C* **124**, 19375 (2020).
29. M.H. Yükselici. Growth kinetics of CdSe nanoparticles in glass. *J. Phys.: Condens. Matter* **14**, 1153 (2002).
30. Yu.M. Azhniuk, V.V. Lopushansky, A.V. Gomonnai, V.O. Yukhymchuk, I.I. Turok, Ya.I. Studenyak. Spectroscopic studies of thermal treatment effect on the composition and size of $CdS_{1-x}Se_x$ nanocrystals in borosilicate glass. *J. Phys. Chem. Solids* **69**, 139 (2008).
31. O. Stroyuk. *Solar Light Harvesting with Nanocrystalline Semiconductors* (Springer, 2018) [ISBN: 978-3-319-68879-4].
32. O. Stroyuk, A. Raevskaya, F. Spranger, O. Selyshchev, V. Dzhagan, D. Solonenko, N. Gaponik, D.R.T. Zahn, A. Eychmüller. Mercury-indium-sulfide nanocrystals: A

new member of the family of ternary In-based chalcogenides. *J. Chem. Phys.* **151**, 144701 (2019).
33. L. Li, T.J.T. Daou, I. Texier, T.K. Chi, T.T. Kim Chi, N.Q. Liem, P. Reiss. Highly luminescent $CuInS_2$/ZnS core/shell nanocrystals: cadmium-free quantum dots for in vivo imaging. *Chem. Mater.* **21**, 2422 (2009).
34. M. Uehara, K. Watanabe, Y. Tajiri, H. Nakamura, H.J. Maeda. Synthesis of $CuInS_2$ fluorescent nanocrystals and enhancement of fluorescence by controlling crystal defect. *Chem. Phys.* **129**, 134709 (2008).
35. Y. Hamanaka, T. Kuzuya, T. Sofue, T. Kino, K. Ito, K. Sumiyama. Defect-induced photoluminescence and third-order nonlinear optical response of chemically synthesized chalcopyrite $CuInS_2$ nanoparticles. *Chem. Phys. Lett.* **466**, 176 (2008).
36. A.E. Raevskaya, O.L. Stroyuk, S.Ya. Kuchmy. Nanoparticles of Ag–In–S and Cu–In–S in aqueous media: preparation, spectral and luminescent properties. *Theor. Experim. Chem.* **53**, 338 (2017).
37. O. Stroyuk, V. Dzhagan, A. Raevskaya, F. Spranger, N. Gaponik, D.R.T. Zahn. Insights into different photoluminescence mechanisms of binary and ternary aqueous nanocrystals from the temperature dependence: A case study of CdSe and Ag–In–S. *J. Lumin.* **215**, 116630 (2019).
38. E. Dutková, M.J. Sayagués, J. Briančin, A. Zorkovská, Z. Bujňáková, J. Kováč, J. Kováč Jr., P. Baláž, J. Ficeriová. Synthesis and characterization of $CuInS_2$ nanocrystalline semiconductor prepared by high-energy milling. *J. Mater. Sci.* **51**, 1978 (2016).
39. S. Sugan, K. Baskar, R. Dhanasekaran. Hydrothermal synthesis of chalcopyrite $CuInS_2$, $CuInSe_2$ and $CuInTe_2$ nanocubes and their characterization. *Curr. Appl. Phys.* **14**, 1416 (2014).
40. P. Scherrer. Bestimmung der Größe und der inneren struktur von kolloidteilchen mittels Röntgenstrahlen. *Nachr. Ges. Wiss. Göttingen, Math. – Phys. Klasse.* **1918**, 98 (1918).
41. D. Li, Y. Zou, D. Yang. Controlled synthesis of luminescent $CuInS_2$ nanocrystals and their optical properties. *J. Lumin.* **132**, 313 (2012).
42. J. Li, B. Kempken, V. Dzhagan, D.R.T. Zahn, J. Grzelak, S. Mackowski, J. Parisi, J. Kolny-Olesiak. Alloyed $CuInS_2$–ZnS nanorods: Synthesis, structure and optical properties. *Cryst. Eng. Comm.* **17**, 5634 (2015).
43. H. Azimi, S. Kuhri, M.S. Stahl, Y. Hou, D.M. Guldi, C.J. Brabec. Elucidating the excited-state properties of $CuInS_2$ nanocrystals upon phase transformation: Quasi-quantum dots versus bulk behavior. *Adv. Electron. Mater.* **1**, 1500040 (2015).
44. V. Dzhagan, B. Kempken, M.Ya. Valakh, J. Parisi, J. Kolny-Olesiak, D.R.T. Zahn. Probing the structure of $CuInS_2$–ZnS core-shell and similar nanocrystals by Raman spectroscopy. *Appl. Surf. Sci.* **395**, 24 (2017).
45. V. Dzhagan, O. Selyshchev, O. Raievska, O. Stroyuk, L. Hertling, N. Mazur, M.Ya. Valakh, D.R.T. Zahn. Phonon spectra of strongly luminescent nonstoichiometric Ag–In–S, Cu–In–S, and Hg–In–S nanocrystals of small size. *J. Phys. Chem. C* **124**, 15511 (2020).
46. J. Alvarez-García, A. Pérez-Rodríguez, A. Romano-Rodríguez, пїS.T. Jawhari, J.R. Morante, R. Scheer, W. Calvet. Raman scattering structural evaluation of $CuInS_2$ thin films. *Thin Solid Films* **387**, 216 (2001).
47. K. Wu, D. Wang. Temperature-dependent Raman investigation of $CuInS_2$ with mixed phases of chalcopyrite and CuAu. *Phys. Status Solidi A* **208**, 2730 (2011).
48. R. Guan, X. Wang, Q. Sun. Structural and optical properties of $CuInS_2$ thin films prepared by magnetron sputtering and sulfurization heat treatment. *J. Nanomater.* **2015**, 579489 (2015).
49. J.K. Larsen, K.V. Sopiha, C. Persson, C. Platzer-Björkman, M. Edoff. Experimental and theoretical study of stable and metastable phases in sputtered $CuInS_2$. *Adv. Sci.* **9**, 2200848 (2022).
50. R. Bacewicz, W. Gębicki, J. Filipowicz. Raman scattering in $CuInS_{2x}Se_{2(1-x)}$ mixed crystals. *J. Phys.: Condens. Matter* **6**, L777 (1994).
51. K. Wakita, H. Hirooka, S. Yasuda, F. Fujita, N. Yamamoto. Resonant Raman scattering and luminescence in $CuInS_2$ crystals. *J. Appl. Phys.* **83**, 443 (1998).
52. F.W. Ohrendorf, H. Haeuseler. Lattice dynamics of chalcopyrite type compounds. Part I. Vibrational frequencies. *Cryst. Res. Technol.* **34**, 339 (1999).
53. I.H. Choi, D.H. Lee. Resonance Raman scattering and exciton-phonon interactions in $CuInS_2$. *J. Kor. Phys. Soc.* **44**, 1542 (2004).
54. V. Dzhagan, A.P. Litvinchuk, M.Y. Valakh, D.R.T. Zahn. Phonon Raman spectroscopy of nanocrystalline multinary chalcogenides as a probe of complex lattice structures. *J. Phys.: Condens. Matter* **35**, 103001 (2023).
55. A.V. Gomonnai, Yu.M. Azhniuk, V.O. Yukhymchuk, M. Kranjčec, V.V. Lopushansky. Confinement-, surface- and disorder-related effects in the resonant Raman spectra of nanometric $CdS_{1-x}Se_x$ crystals. *Phys. Stat. Solidi B* **239**, 490 (2003).
56. V.M. Dzhagan, M.Ya. Valakh, A.E. Raevskaya, A.L. Stroyuk, S.Ya. Kuchmiy, D.R.T. Zahn. Size effects on Raman spectra of small CdSe nanoparticles in polymer films. *Nanotechnology* **19**, 305707 (2008).
57. V. Izquierdo-Roca, X. Fontané, E. Saucedo, J.S. Jaime-Ferrer, J. Álvarez-García, A. Pérez-Rodríguez, V. Bermudez, J.R. Morante. Process monitoring of chalcopyrite photovoltaic technologies by Raman spectroscopy: an application to low cost electrodeposition based processes. *New J. Chem.* **35**, 453 (2011).
58. K. Kambas, J. Spyridelis, M. Balkanski. Far-infrared and Raman optical study of α- and β-In_2S_3 compounds. *Phys. Status Solidi B* **105**, 291 (1981).
59. O. Surucu, M. Isik, M. Terlemezoglu, N.M. Gasanly, M. Parlak. Structural and temperature-tuned bandgap characteristics of thermally evaporated β-In_2S_3 thin films. *J. Mater. Science: Mater. in Electronics* **32**, 15851 (2021).

60. Ye. Havryliuk, M.Ya. Valakh, V. Dzhagan, O. Greshchuk, V. Yukhymchuk, A. Raevskaya, O. Stroyuk, O. Selyshchev, N. Gaponik, D.R.T. Zahn. Raman characterization of Cu_2ZnSnS_4 nanocrystals: phonon confinement effect and formation of Cu_xS phases. *RSC Adv.* **8**, 30736 (2018).
61. A. Kasuya, K. Watanabe, H. Takahashi, K. Toji, K. Motomiya, Y. Nishina. Stability of S_xSe_y ring clusters studied by Raman scattering. *Mater. Sci. Eng. A* **217–218**, 12 (1996).
62. F. Kyriazis, S.N. Yannopoulos. Colossal photostructural changes in chalcogenide glasses: Athermal photoinduced polymerization in As_xS_{100-x} bulk glasses revealed by near-bandgap Raman scattering. *Appl. Phys. Lett.* **94**, 101901 (2009).
63. L. Borkovska, A. Romanyuk, V. Strelchuk, Y. Polishchuk, V. Kladko, O. Stroyuk, A. Raevskaya, T. Kryshtab. The photoluminescence properties of $CuInS_2$ and $AgInS_2$ nanocrystals synthesized in aqueous solutions. *ECS Transactions* **66**, 171 (2015).
64. B.V. Lopushanska, Y.M. Azhniuk, I.P. Studenyak, V.V. Lopushansky, A.V. Gomonnai, D.R.T. Zahn. Optical characterization of colloidal $AgInS_2$ quantum dots synthesized from aqueous solutions. *J. Nano- and Electron. Phys.* **14**, 04010 (2022).
65. Y. Azhniuk, B. Lopushanska, O. Selyshchev, Y. Havryliuk, A. Pogodin, O. Kokhan, A. Ehm, V. Lopushansky, I. Studenyak, D.R.T. Zahn. Synthesis and optical properties of Ag–Ga–S quantum dots. *Phys. Status Solidi B* **259**, 2100349 (2022).

Received 10.04.23

Ю.М. Ажнюк, Є.О. Гаврилюк, Б.В. Лопушанська, В.В. Лопушанський, О.В. Гомоннай, Д.Р.Т. Цан

СТРУКТУРНІ Й ОПТИЧНІ ХАРАКТЕРИСТИКИ РОЗПОДІЛЕНИХ ЗА РОЗМІРОМ КВАНТОВИХ ТОЧОК Cu–In–S, ВКРИТИХ ГЛУТАТІОНОМ

Реакцією обміну у водних розчинах при помірних умовах синтезу отримано розподілені за розміром серії збіднених міддю колоїдних квантових точок (КТ) Cu–In–S, стабілізованих глутатіоном. Ширина оптичної забороненої зони та спектральне положення максимуму фотолюмінесценції зміщуються в бік вищих енергій зі зменшенням розміру КТ. На основі даних дифракції рентгенівських променів показано, що КТ характеризуються тетрагональною структурою типу халькопіриту. Середні розміри КТ, оцінені за формулою Шерера, а також знайдені за розмірними кривими, побудованими на основі спектрів поглинання, непогано узгоджуються між собою (в інтервалі 1,2–2,9 нм). Проаналізовано раманівські спектри КТ Cu–In–S з урахуванням їхньої структури, ефектів, пов'язаних з просторовим обмеженням, відхилення від стехіометрії та можливого існування вторинних фаз.

Ключові слова: квантові точки, колоїдний синтез, оптичне поглинання, фотолюмінесценція, дифракція рентгенівських променів, раманівська спектроскопія.